Integrated Modeling, Finite-Element Analysis, and Engineering Design for Thin-Shell Structures using Subdivision

Fehmi Cirak, Michael J. Scott, Erik K. Antonsson,
Michael Ortiz and Peter Schröder

Division of Engineering and Applied Science, California Institute of Technology, Pasadena, CA 91125, U.S.A.

Abstract

Many engineering design applications require geometric modeling and mechanical simulation of thin flexible structures, such as those found in the automotive and aerospace industries. Traditionally, geometric modeling, mechanical simulation, and engineering design are treated as separate modules requiring different methods and representations. Due to the incompatibility of the involved representations the transition from geometric modeling to mechanical simulation, as well as in the opposite direction, requires substantial effort. However, for engineering design purposes efficient transition between geometric modeling and mechanical simulation is essential. We propose the use of subdivision surfaces as a common foundation for modeling, simulation, and design in a unified framework. Subdivision surfaces provide a flexible and efficient tool for arbitrary topology free-form surface modeling, avoiding many of the problems inherent in traditional spline patch based approaches. The underlying basis functions are also ideally suited for a finite-element treatment of the so-called thin shell equations, which describe the mechanical behavior of the modeled structures. The resulting solvers are highly scalable, providing an efficient computational foundation for design exploration and optimization. We demonstrate our claims with several design examples, showing the versatility and high accuracy of the proposed method.

Key words: Subdivision Surfaces; Finite-Elements; Shells;

1 Introduction

Current engineering design practice in industry employs a sequence of tools which are generally not well matched to each other. For example, the output of a computer aided geometric design (CAGD) system is typically not suitable

as direct input for a finite-element modeler. This is usually addressed through intermediate tools such as mesh generators. Unfortunately, these are notoriously lacking in robustness. Even once a geometric model has been successfully meshed, the output of a finite-element simulation cannot be directly applied to the original geometric model, since there is no straightforward mapping back to the original design degrees of freedom. Additionally there is a need for a trade-off between the speed of analysis and the fidelity of the results. In the early stages of design, quick results are necessary, but approximate results are acceptable. In the later stages, highly precise results are required, and longer computation times are tolerated. Worse, different underlying models are required for each level of refinement. These difficulties make the design process cumbersome and inhibit rapid iteration over design alternatives (Figure 1). Many of these difficulties can be greatly reduced in a unified representation paradigm, *e.g.*, an environment in which the geometric model uses the same underlying representation as the appropriate finite-element simulation. The principal advantage of such a unified representation paradigm is the simple and rapid data transfer between the geometric design and finite-element analysis tools. No cumbersome remodeling of already generated geometric models for purposes of finite-element simulation is required. As a result the investigation of different design alternatives, *e.g.*, for design space exploration, will be substantially simplified. In applications this will lead to faster product development cycles through the tight combination of the design and analysis steps. Historically modeling and simulation tools were developed in different communities with limited interactions. To our knowledge few attempts have been made in the past to unify geometric modeling and simulation based on a common representation paradigm (14; 17). Our contribution in this paper is to demonstrate a computationally simple and theoretically well-justified framework for an *integrated* treatment of free-form geometric modeling and finite-element analysis of thin-shells for purposes of engineering design.

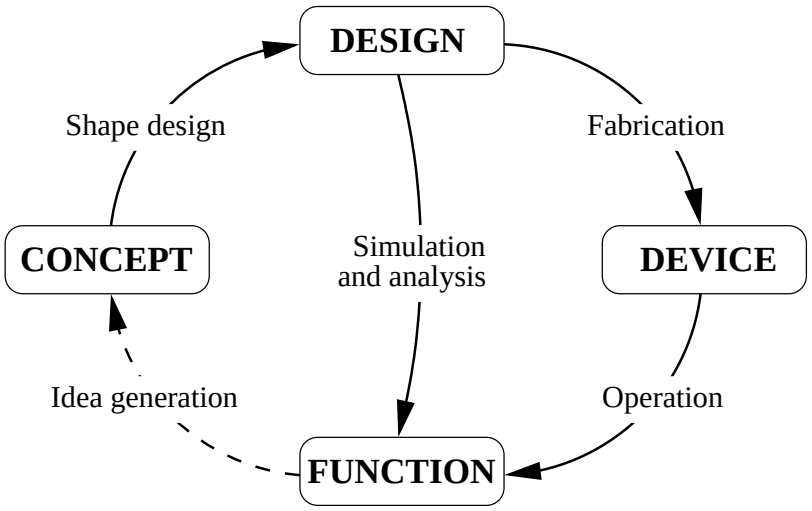

Fig. 1. Iteration cycle in the product development.

Thin flexible structures (plates and shells) appear in many areas of applied engineering design, *e.g.*, in the automobile and aerospace industries. As the underlying representation for such structures we have chosen subdivision surfaces. It is well known that they have many practical advantages for free-form geometric modeling, in particular for shapes of arbitrary topology. With the recent development of subdivision algorithms supporting such important modeling operations as trimming, boundary interpolation, and description of small features (4; 16; 19), subdivision surfaces are well positioned to become a fundamental modeling primitive for CAGD applications (2).

Additionally, it has recently been demonstrated (8; 7) that the basis functions induced by subdivision, when used as shape functions in the finite-element method, have *significant* advantages over the previous state of the art in the numerical simulation of thin shells. Similar to a thin-*plate*, the deformation of curved *shells* is described by partial differential equations with derivatives up to order four, requiring shape functions with square integrable curvatures for finite-element treatments. The choice of subdivision shape functions can be contrasted with more traditional approaches for the construction of shape functions, which are typically based on Hermite interpolation. It is well known that this leads to fifth order polynomials over triangles. Higher order shape functions, however, are not suitable for practical problems with such features as reentrant corners, jumps in the material properties, or point loads, which exhibit singularities in the exact solution. Subdivision surfaces satisfy the necessary analytic requirements (27) while being parameterized strictly in terms of displacements only and circumvent the usual difficulties with traditional finite-element treatments.

The many advantages of the subdivision method for geometric modeling *and* for mechanical simulation makes it a method of choice for integrated design and simulation. The need to convert an existing CAD model to a finite-element mesh and the difficulty of doing so robustly is entirely circumvented. Since the finite-element solver uses the same degrees of freedom as the free-form geometric modeling system, optimization of the geometry based on the results of mechanics simulations is immediate. The latter in particular greatly facilitates the iterative process of engineering design.

1.1 Overview

Section 2 serves mainly to recall some facts about subdivision and to establish notation. While we restrict our framework to Loop surfaces (20) in the present paper we hasten to point out that the basic algorithms are equally applicable to other subdivision schemes, in particular the scheme of Catmull and Clark (6). Section 3 recalls the basic formulation of the equations govern-

ing the mechanical behavior of thin flexible structures. Detailed derivations, convergence studies, and more sophisticated material models are described elsewhere (8; 7). Finally, Section 4 discusses a basic framework for design space exploration and presents an integrated framework for modeling, simulation and design with subdivision surfaces. Two engineering design examples (square plate and car hood) are used to demonstrate the proposed approach.

2 Subdivision Surfaces

Subdivision schemes construct smooth surfaces through a limiting procedure of repeated refinement starting from an initial control mesh (Figure 2). They were first proposed in 1978 by Catmull and Clark (6) and Doo and Sabin (9) to address some of the shortcomings of traditional spline patches when modeling arbitrary topology surfaces. Since then many other schemes have been proposed and studied (for an overview the interested reader is referred to (37) and the references therein). For purposes of free-form geometric modeling with concurrent thin-shell finite-element analysis, subdivision methods which result in limit surfaces whose curvature tensor is square integrable are especially appealing.

For our purposes we have chosen the triangle-based, primal, approximating scheme of Loop (20), which generalizes the three direction quartic box-spline to arbitrary topology control meshes. For almost all initial control meshes, the resulting surfaces are C^2 except at irregular vertices where the surfaces are C^1 only. In the case of triangle based subdivision all interior vertices of valence other than 6 as well as boundary vertices of valence other than 4 are referred to as irregular. While the curvatures at irregular vertices diverges, the curvatures are square integrable (27) as required for thin-shell analysis. A detailed description of the Loop subdivision rules including the treatment of boundaries, convex and concave corners, as well as tangent plane boundary conditions can be found in (4).

For later use we fix notation as follows. Each vertex of the control mesh has associated with it a point position in three space, sometimes also referred to as "nodal position" (in analogy to the term traditionally used in the finite-element literature). Vertices are indexed by some integer set $l = \{0, \ldots, L\}$ and the associated nodal position is $\boldsymbol{x}_l$.

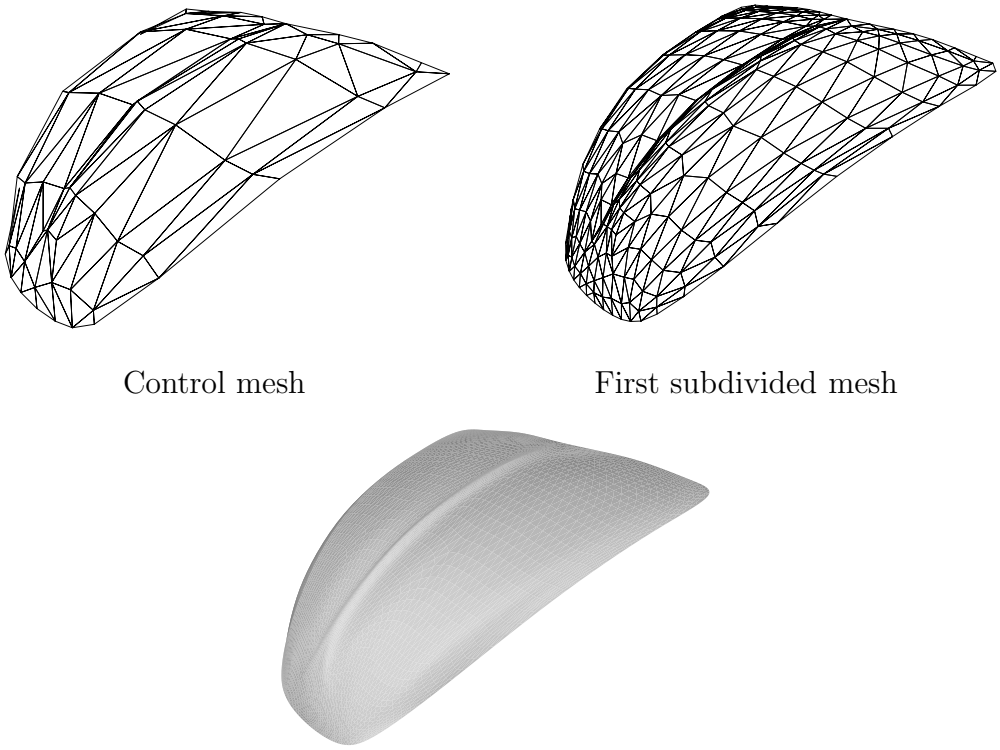

Control mesh First subdivided mesh

Limit surface

Fig. 2. Subdivision describes a smooth surface as the limit of a sequence of refined polyhedra.

2.1 Limit Surface Evaluation

In order to apply the finite-element method to subdivision surfaces we need to have a proper parameterization of the surface in terms of elementary domain elements. The natural choice are the triangles of the control mesh, each of which can be treated as a subset of the domain and brought into correspondence with a "master element" (Figure 3). Additionally, efficient evaluation routines for limit surface quantities such as first and second derivatives need to be available. General methods for this task were first described by Stam (32; 31). However, we are interested only in specific parameter values, namely those needed for quadrature evaluation of stiffness integrals arising from the computation of the mechanical response of the surface. For this the fully general method is not needed. In particular one-point, barycenter based quadratures are sufficient (8).

A convenient local parameterization of the limit surface may be obtained as follows. For each triangle in the control mesh we choose (θ^1, θ^2) as two of its barycentric coordinates within their natural range:

$$T = \{(\theta^1, \theta^2),\ \text{s. t. } \theta^\alpha \in [0,1],\ 0 \leq \theta^1 + \theta^2 \leq 1\}$$

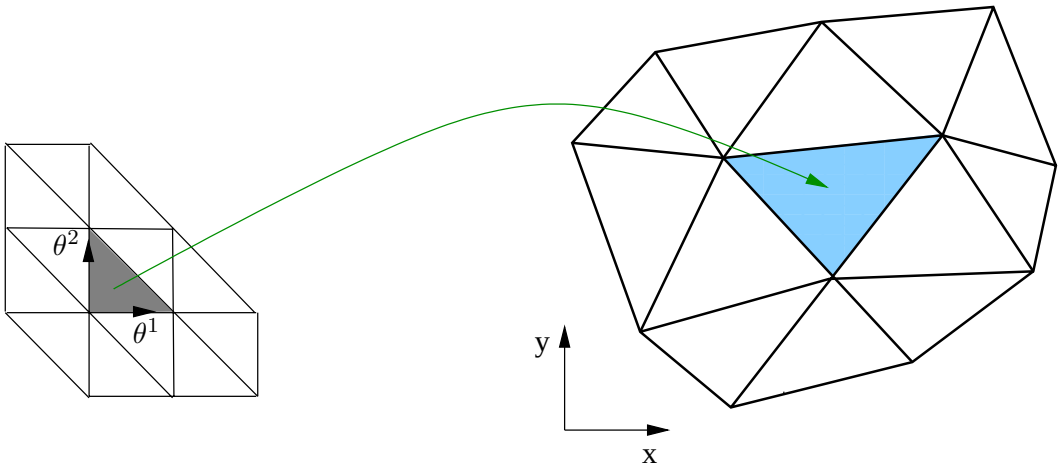

Fig. 3. Master element (left) and the control mesh (right).

The triangle T in the (θ^1, θ^2)-plane may be regarded as a master or standard element domain. It should be emphasized that this parameterization is defined locally for each element in the mesh. The entire discussion of parameterization and function evaluation may therefore be couched in local terms.

In the regular setting the scheme of Loop leads to quartic box-splines. Therefore, the local parameterization of the limit surface may be expressed in terms of box-spline shape functions, with the result:

$$\boldsymbol{x}(\theta^1, \theta^2) = \sum_{l=1}^{12} N^l(\theta^1, \theta^2)\boldsymbol{x}_l \tag{1}$$

where now the labels l refer to the *local* numbering of the nodes (all nodes shown in Figure 3). The precise form of the shape functions $N^l(\theta^1, \theta^2)$ is given in the companion paper (8). The embedding (eq. 1) may thus be regarded as a conventional isoparametric mapping from the standard domain T onto the limit surface Ω, with (θ^1, θ^2) playing the role of natural coordinates.

For function evaluation on irregular patches, *i.e.*, those with one or more irregular vertices incident, the mesh has to be subdivided until the parameter value of interest is interior to a regular patch. At that point the regular box spline parameterization applies once again. It should be noted that the refinement is performed for parameter evaluation only. For simplicity we assume that irregular patches have one irregular vertex only. This restriction can always be met for arbitrary initial meshes through one step of subdivision, which has the effect of separating all irregular vertices. As shown in Figure 4, after one subdivision step the triangles marked one, two, and three are regular patches. The action of the subdivision operator for this entire neighborhood can be described by a matrix:

$$\boldsymbol{X}^1 = \boldsymbol{A}\boldsymbol{X}^0$$

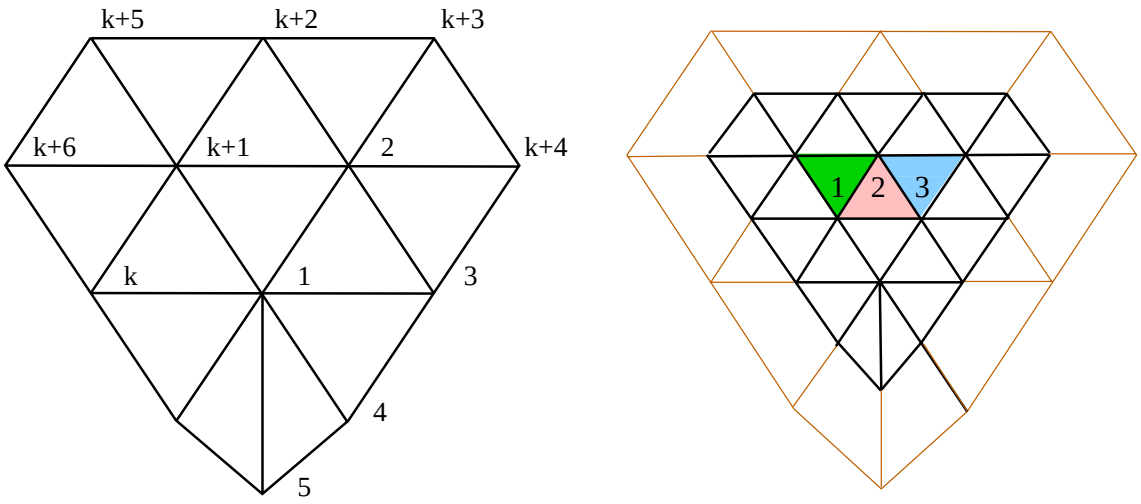

Fig. 4. Refinement near an irregular vertex.

The matrix $\boldsymbol{A}$ has dimension $(k+12,\ k+6)$ and its entries can be derived from the subdivision rules. For the proposed shell element with one point quadrature at the barycenter of the master element, a single subdivision step is sufficient, since the sampling point (center of the initial patch) lies in sub-patch 2. We define 12 selection vectors $\boldsymbol{P}_l, l = 1, \ldots, 12$ of dimension $(k+12)$ which extract the 12 box-spline control points for sub-patch 2 from the $k+12$ points of the refined mesh. The entries of $\boldsymbol{P}_l$ are zero and one depending on the indices of the initial and refined meshes. To evaluate the function values in the three triangles with the box-spline shape functions N^l, a coordinate transformation must be performed. The relation between the coordinates (θ^1, θ^2) of the original triangles and the coordinates $(\tilde{\theta^1}, \tilde{\theta^2})$ of the refined triangles can be established from the refinement pattern in Figure 5. For the sub-patch 2 we have the following relation:

$$\text{Triangle 2:}\quad \tilde{\theta^1} = 1 - 2\theta^1 \qquad \text{and} \qquad \tilde{\theta^2} = 1 - 2\theta^2$$

The function values and derivatives for sub-patch 2 can now be evaluated

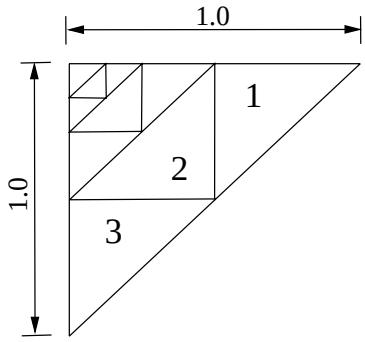

Fig. 5. Refinement of the master triangle.

using the interpolation rule:

$$\boldsymbol{x}(\theta^1, \theta^2) = \sum_{l=1}^{12} N^l(\tilde{\theta^1}, \tilde{\theta^2}) \boldsymbol{P}_l \boldsymbol{A} \boldsymbol{X}^0 \tag{2}$$

Derivatives, required for instance for the computation of the potential energy, follow by direct differentiation of the interpolation rule (eq. 2).

3 Review of Thin-Shell Equations

The mechanical response of a subdivision surface with an attached thickness property can be computed with the classical Kirchhoff-Love shell theory. In this section we briefly summarize the resulting field equations. A detailed presentation of classical shell theories can be found in (23). The final result of our derivation will be couched in terms of constrained energy minimization where the internal energy of the shell depends on invariant quantities of the surface such as the metric and curvature tensor.

3.1 Related Methods in Geometric Modeling

Before going into the details of the description of the mechanical behavior of shells, it is useful to briefly contrast our approach with other energy minimization methods. These often appear in variational modeling. For example, Halstead, *et al.* (12) described an algorithm for fair interpolation of a given set of points with a Catmull-Clark surface. To constrain the solution space they search for a parameterized surface $\boldsymbol{x}$ which simultaneously interpolates the given constraints and minimizes an energy functional Φ over the domain Ω based on a weighted average of squared first and second derivatives:

$$\Phi[\boldsymbol{x}] = \alpha \int_\Omega (\boldsymbol{x}_{,1})^2 + (\boldsymbol{x}_{,2})^2 d\Omega + \beta \int_\Omega (\boldsymbol{x}_{,11})^2 + 2(\boldsymbol{x}_{,12})^2 + (\boldsymbol{x}_{,22})^2 d\Omega$$

where α and β are some prescribed constants and a comma is used to denote partial differentiation. These terms are sometimes referred to as stretching and bending energies. While such formulations are typically derived from a thin-*plate* ansatz they cannot describe the mechanical behavior of a shell correctly since the result of the computation depends on the particular parameterization chosen. In fact using the standard parameterization leads to infinite bending energies (12) and either zero or infinite stretching energies near irregular vertices. Such methods can nonetheless be useful for scattered data interpolation

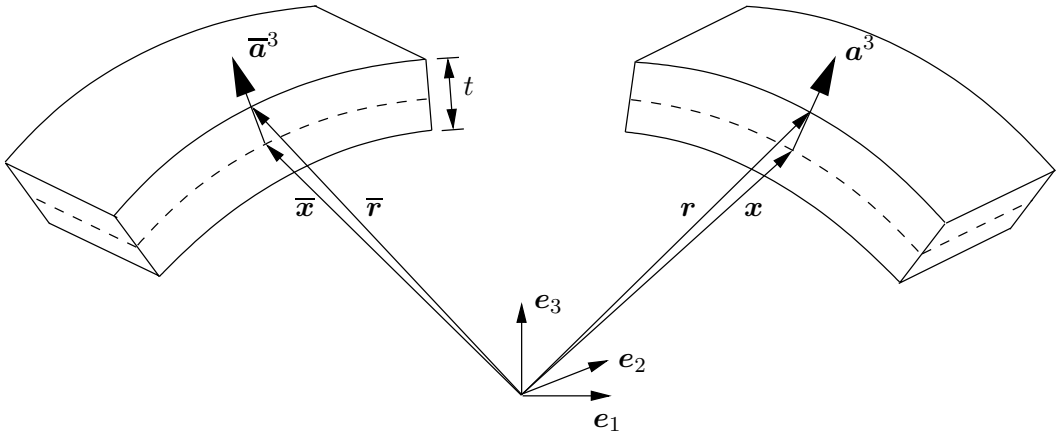

Fig. 6. Shell geometry in the reference (left) and the deformed (right) configurations.

after suitable modifications near the extraordinary vertices (21) or elimination of the infinite energy modes (12). To accurately and consistently describe the mechanical behavior of shells a formulation in terms of intrinsic surface properties is required.

3.2 Kinematics of Deformation

We begin by considering a shell whose undeformed middle surface is characterized by a subdivision surface of domain $\overline{\Omega}$ and boundary $\overline{\Gamma} = \partial\overline{\Omega}$. The shell deforms under the action of applied loads and adopts a deformed middle surface characterized by a surface of domain Ω and boundary $\Gamma = \partial\Omega$. The position vectors $\overline{\boldsymbol{r}}$ and $\boldsymbol{r}$ of a material point in the reference and deformed configurations of the shell may be parameterized in terms of a system of curvilinear coordinates $\{\theta^1, \theta^2, \theta^3\}$ as:

$$\overline{\boldsymbol{r}}(\theta^1, \theta^2, \theta^3) = \overline{\boldsymbol{x}}(\theta^1, \theta^2) + \theta^3 \overline{\boldsymbol{a}}_3(\theta^1, \theta^2) \quad -\frac{t}{2} \leq \theta^3 \leq \frac{t}{2}$$

and

$$\boldsymbol{r}(\theta^1, \theta^2, \theta^3) = \boldsymbol{x}(\theta^1, \theta^2) + \theta^3 \boldsymbol{a}_3(\theta^1, \theta^2) \quad -\frac{t}{2} \leq \theta^3 \leq \frac{t}{2}$$

The functions $\overline{\boldsymbol{x}}(\theta^1, \theta^2)$ and $\boldsymbol{x}(\theta^1, \theta^2)$ furnish a parametric representation of the middle surface of the shell in the reference and deformed configurations, respectively, while t gives the thickness of the surface (Fig. 6). The corresponding surface basis vectors are:

$$\overline{\boldsymbol{a}}_\alpha = \overline{\boldsymbol{x}}_{,\alpha} \quad \text{and} \quad \boldsymbol{a}_\alpha = \boldsymbol{x}_{,\alpha}$$

where the comma is used to denote partial differentiation with respect to θ^α and the Greek indices take the value 1 and 2. The shell directors $\overline{\boldsymbol{a}}_3$ and $\boldsymbol{a}_3$ are the unit normal vectors to the undeformed and deformed shell middle surfaces, respectively. The covariant components of the surface metric tensors in turn follow as:

$$\overline{a}_{\alpha\beta} = \overline{\boldsymbol{a}}_\alpha \cdot \overline{\boldsymbol{a}}_\beta \quad \text{and} \quad a_{\alpha\beta} = \boldsymbol{a}_\alpha \cdot \boldsymbol{a}_\beta$$

whereas the covariant components of the curvature tensors are given by:

$$\overline{\kappa}_{\alpha\beta} = -\overline{\boldsymbol{a}}_{\alpha,\beta} \cdot \overline{\boldsymbol{a}}_3 \quad \text{and} \quad \kappa_{\alpha\beta} = -\boldsymbol{a}_{\alpha,\beta} \cdot \boldsymbol{a}_3$$

We define the following two strain measures for describing the change in the geometry between reference and the deformed geometry:

$$\alpha_{\alpha\beta} = \frac{1}{2}(a_{\alpha\beta} - \overline{a}_{\alpha\beta}) \quad \text{and} \quad \beta_{\alpha\beta} = \kappa_{\alpha\beta} - \overline{\kappa}_{\alpha\beta}$$

In particular, the in-plane components $\alpha_{\alpha\beta}$, or membrane strains, measure the straining of the surface and the components $\beta_{\alpha\beta}$, or bending strains, measure the bending or change in curvature of the shell. The linearized membrane and bending strains are of the form:

$$\alpha_{\alpha\beta} = \frac{1}{2}(\overline{\boldsymbol{a}}_\alpha \cdot \boldsymbol{u}_{,\beta} + \boldsymbol{u}_{,\alpha} \cdot \overline{\boldsymbol{a}}_\beta) \tag{3}$$

and

$$\begin{aligned}\beta_{\alpha\beta} = &-\boldsymbol{u}_{,\alpha\beta} \cdot \overline{\boldsymbol{a}}_3 + \frac{1}{\sqrt{\overline{a}}}\left[\boldsymbol{u}_{,1} \cdot (\overline{\boldsymbol{a}}_{\alpha,\beta} \times \overline{\boldsymbol{a}}_2) + \boldsymbol{u}_{,2} \cdot (\overline{\boldsymbol{a}}_1 \times \overline{\boldsymbol{a}}_{\alpha,\beta})\right] \\ &+ \frac{\overline{\boldsymbol{a}}_3 \cdot \overline{\boldsymbol{a}}_{\alpha,\beta}}{\sqrt{\overline{a}}}\left[\boldsymbol{u}_{,1} \cdot (\overline{\boldsymbol{a}}_2 \times \overline{\boldsymbol{a}}_3) + \boldsymbol{u}_{,2} \cdot (\overline{\boldsymbol{a}}_3 \times \overline{\boldsymbol{a}}_1)\right]\end{aligned} \tag{4}$$

It is clear from these expressions that the middle surface displacement field $\boldsymbol{u} = \boldsymbol{x} - \overline{\boldsymbol{x}}$ furnishes a complete description of the shell deformation and may therefore be regarded as the primary unknown of the analysis.

3.3 Weak Form of Equilibrium and Discretization

The potential energy of the shell has the form:

$$\Phi[\boldsymbol{u}] = \int_{\overline{\Omega}} W(\boldsymbol{u})\, d\overline{\Omega} + \Phi_{\text{ext}} = \Phi_{\text{int}} + \Phi_{\text{ext}}$$

where Φ_{int} is the elastic energy and Φ_{ext} is the potential of the applied loads. For simplicity, we shall assume throughout that the shell is linearly elastic with strain energy density per unit area of the form:

$$W(\boldsymbol{u}) = \frac{1}{2}\frac{Et}{1-\nu^2}H^{\alpha\beta\gamma\delta}\alpha_{\alpha\beta}\alpha_{\gamma\delta} + \frac{1}{2}\frac{Et^3}{12(1-\nu^2)}H^{\alpha\beta\gamma\delta}\beta_{\alpha\beta}\beta_{\gamma\delta} \tag{5}$$

whereby the Einstein summation convention applies, ν denotes Poisson's ratio and E denotes Young's modulus (10). The fourth order constitutive tensor $H^{\alpha\beta\gamma\delta}$ is given by

$$H^{\alpha\beta\gamma\delta} = \nu\,\overline{a}^{\alpha\beta}\overline{a}^{\gamma\delta} + \frac{1}{2}(1-\nu)\,(\overline{a}^{\alpha\gamma}\overline{a}^{\beta\delta} + \overline{a}^{\alpha\delta}\overline{a}^{\beta\gamma}) \tag{6}$$

with the contravariant components of the surface metric tensor $\overline{a}^{\alpha\beta}$. In (eq. 5), the first term is the membrane strain energy density and the second term is the bending strain energy density.

The stable equilibrium configurations of the shell now follow from the principle of minimum potential energy. The Euler-Lagrange equations corresponding to the minimum principle may be expressed in weak form as:

$$\langle D\Phi[\boldsymbol{u}], \boldsymbol{v}\rangle = \langle D\Phi_{\text{int}}[\boldsymbol{u}], \boldsymbol{v}\rangle + \langle D\Phi_{\text{ext}}[\boldsymbol{u}], \boldsymbol{v}\rangle = 0 \tag{7}$$

where $\boldsymbol{v}$ is the trial displacement field. In particular, the internal energy has the form:

$$\begin{aligned}\langle D\Phi_{\text{int}}[\boldsymbol{u}], \boldsymbol{v}\rangle = \int_{\overline{\Omega}} [&\frac{Et}{1-\nu^2}H^{\alpha\beta\gamma\delta}\alpha_{\alpha\beta}(\boldsymbol{u})\alpha_{\gamma\delta}(\boldsymbol{v}) + \\ &\frac{Et^3}{12(1-\nu^2)}H^{\alpha\beta\gamma\delta}\beta_{\alpha\beta}(\boldsymbol{u})\beta_{\gamma\delta}(\boldsymbol{v})]d\overline{\Omega}\end{aligned}$$

It is clear that the displacements $\boldsymbol{u}$ and the trial functions $\boldsymbol{v}$ must necessarily have square integrable first and second derivatives. Under suitable technical restrictions on the domain $\overline{\Omega}$ and the applied loads, it therefore follows that the displacements and the trial functions have to be in the Sobolev space $H^2(\overline{\Omega}, R^3)$. In particular, an acceptable finite-element interpolation method must guarantee that all interpolants belong to this space. Next we proceed to partition the domain $\overline{\Omega}$ of the shell middle surface into a set of elements as induced by the original control mesh. The collection of element domains in the mesh is $\{\overline{\Omega}_j,\ j = 1, \ldots, n\}$, where $\overline{\Omega}_j$ denotes the domain of element j and n is the total number of elements in the domain. The control mesh may

be taken as a basis for introducing interpolants of the general form:

$$\overline{\boldsymbol{x}}_h(\theta^1,\theta^2)=\sum_{l=1}^{L}N^l(\theta^1,\theta^2)\overline{\boldsymbol{x}}_l \quad \text{and} \quad \boldsymbol{u}_h(\theta^1,\theta^2)=\sum_{l=1}^{L}N^l(\theta^1,\theta^2)\boldsymbol{u}_l \tag{8}$$

where $\{N^l,\ l=1,\ldots,L\}$ are the shape functions, $\{\overline{\boldsymbol{x}}_l,\ l=1,\ldots,L\}$ are the coordinate vectors of the control points in the reference configuration, $\{\boldsymbol{u}_l,\ l=1,\ldots,L\}$ are the corresponding nodal displacement vectors, and L is the number of nodes in the mesh. Furthermore, the displacement interpolation (eq. 8) inserted in (eqs. 3 and 4) gives the finite-element membrane and bending strains in the form:

$$\boldsymbol{\alpha}_h(\theta^1,\theta^2)=\sum_{l=1}^{L}\boldsymbol{M}^l(\theta^1,\theta^2)\boldsymbol{u}_l \quad \text{and} \quad \boldsymbol{\beta}_h(\theta^1,\theta^2)=\sum_{l=1}^{L}\boldsymbol{B}^l(\theta^1,\theta^2)\boldsymbol{u}_l \tag{9}$$

The exact form of the matrices $\boldsymbol{M}^l$ and $\boldsymbol{B}^l$ can be found in the companion paper (8). Introducing the strain interpolations (eq. 9) into the weak form (eq. 7) and subsequent numerical integration of the integrals leads to the discrete equilibrium equation:

$$\sum_{m=1}^{L}\boldsymbol{K}^{lm}\boldsymbol{u}_m=\boldsymbol{f}^l \tag{10}$$

where $\boldsymbol{K}^{lm}$ is the stiffness matrix and $\boldsymbol{f}^l$ is a force vector.

3.3.1 Remarks

- Theoretical considerations and numerical tests show that a one-point quadrature rule leads to a discrete stiffness matrix with full rank, and optimal convergence of the method. The integration point is at the barycenter of the elements. Sufficient conditions for the quadrature rule to preserve the order of convergence of the finite-element method may be found in (33).
- The derived strain-displacement relations (eqs. 9) and the introduced material model (eq. 6) are linear. The presented theory can thus only be applied in the small displacement and strain regime.
- The extension of the methods to the large deformation case can be found in the companion paper (7).
- The resulting algebraic equation system (eq. 10) is, as usual for finite-element methods, sparse. We solve it with a standard direct method specially tailored for sparse matrices.
- A classical approach to avoid the use of smooth shape functions in finite-element computations is based on the theory of thick-shells with shear defor-

mation (1). The related finite-element implementations require only piecewise continuous shape functions, but lead to problems such as shear locking for thin-shells – especially in the presence of severe element distortion.

4 Design Space Exploration and Multi-Attribute Decision-Making

Engineering design requires a range of analysis methods, such as the subdivision method for thin-shell structural analysis, in order to assess one or more aspects of performance for any particular design candidate. However, several additional elements must also be available to the design engineer to make effective use of such analysis methods. The designer needs:

- some approach to determine or propose which candidates to analyze,
- some method for trading-off cost and fidelity of analysis, and
- a method for trading-off, or aggregating, multiple, usually competing aspects of performance (*e.g.*, mass and stiffness).

The subdivision method for thin-shell structural analysis provides a powerful technique for trading-off cost and fidelity of analysis, by:

- permitting the use of a coarse mesh early in the design procedure when a large number of design alternatives are being considered, and the resources that can be applied to the (preliminary) analysis of any one alternative are small, and
- increasing the fidelity of the analysis, by subdivision of the mesh, as the design process proceeds and the number of design alternatives being considered is reduced, and the resources that can be applied to the analysis of any one alternative grow.

This is particularly beneficial, as the underlying model of the shell does not need to be recreated as the design proceeds; only the degree of subdivision applied to the original model needs to be increased.

The multi-attribute character makes engineering design more than a simple optimization problem. In multi-attribute problems, trade-offs among criteria can play a determining role, and the designer is frequently interested in a Pareto frontier of points (15; 34) rather than a single optimum.

A *Pareto point* is a point in the set of possible designs that matches or exceeds the performance of any other possible design point on at least one attribute; if one point is better than a second on all attributes, the second point is *dominated* and cannot be a Pareto point. The Pareto frontier is the set of Pareto points. A set of Pareto points comprising a Pareto frontier in a discrete

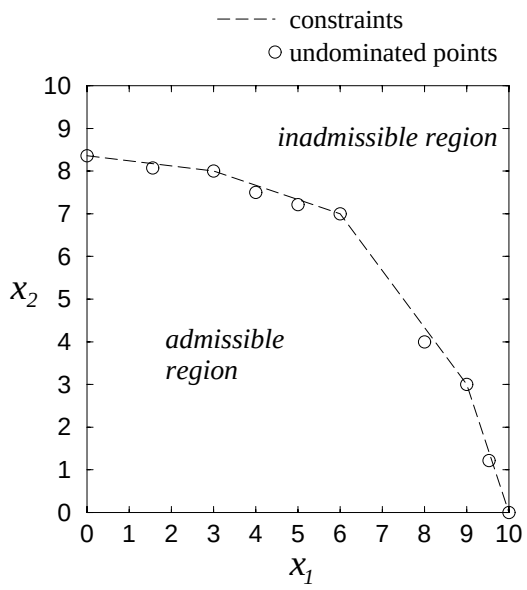

Fig. 7. A Set of Pareto Points.

2-dimensional problem is shown in Figure 7.

The choice of a trade-off strategy (or aggregation) determines which of the undominated (Pareto) points is selected as best satisfying the multiple criteria. Choosing an appropriate trade-off strategy is a crucial part of the engineering design process, principally because it can dramatically affect the result (25). A family of functions, appropriate for engineering design, to perform this aggregation is introduced in (29).

It can be highly beneficial for the engineer to consider *sets* of designs (3). As the design process proceeds, the size of the set of designs under consideration is reduced, and the fidelity of the analysis is increased. Set-based methods have been shown to facilitate design concurrency (35).

The design engineer's task involves proposing alternative solutions, coupled with an iterative exploration of the design space. The dimension of a typical design space may be in the tens or hundreds. Unless the measure of performance is an analytic function of the design variables (an unusual case), the engineer must construct the performance function through pointwise evaluation of the design space. Even for rapid performance calculations, "exhaustive" exploration of a design space (even to a modest resolution in each dimension) is prohibitively expensive; for calculations such as finite-element analysis that may take many minutes of cpu time, even a rudimentary exploration of the design space becomes impossible.

Methods for coping with this computational difficulty at any one level of design resolution include polynomial and other approximations of the performance function (Design of Experiments (22), Kriging (30), MARS (13), Response

Surface methods, local approximation of partial derivatives (sensitivity analysis (18)), directed pointwise search (classical optimization (26)) and *ad hoc* selection guided by experience and intuition.

For multi-attribute problems, decision analysis methods are used to assess the performance of *sets* of designs (the Method of Imprecision (3; 36)), and to trade-off multiple competing aspects of the design (utility theory (15), matrix methods, and aggregation methods (25; 29)).

Finally, engineers routinely use models of differing resolution at different stages of a design process, for example, progressing from linear beam calculations at an early stage of design to a finely-meshed non-linear finite-element analysis when the geometry of the part is more precisely described. Such models cannot be described as *multi-resolution*, however, for the engineer must employ different models to change resolutions.

The subdivision method for thin-shell structural analysis provides a true, natural, multi-resolution analysis, where one model supports many different resolutions. As with other modeling methods, increased fidelity comes at an increased computational cost. However, here the designer specifies a single parameter (the level of subdivision) to choose faster analyses in the early stages and more accurate ones later, rather than building a new model for each desired level of resolution of the same design.

5 Examples

We present two design examples to illustrate the framework presented above for integrated modeling, finite-element analysis and design of thin-shells based on subdivision surfaces. In the examples, the initial design is improved with respect to various objective functions. For optimization we employ a simple pattern search algorithm. The search is based only on the value of the objective function and does not require function derivatives. If derivatives (sensitivities) are available more sophisticated optimization algorithms can be utilized (see, *e.g.*, (11; 24; 5) among many others).

5.1 Square Plate

The first example is the design of a uniformly loaded roof over a square shaped area (Figure 8). The roof is supported at the four corners. The design objective is to maximize the stiffness (or to minimize the compliance) of the structure,

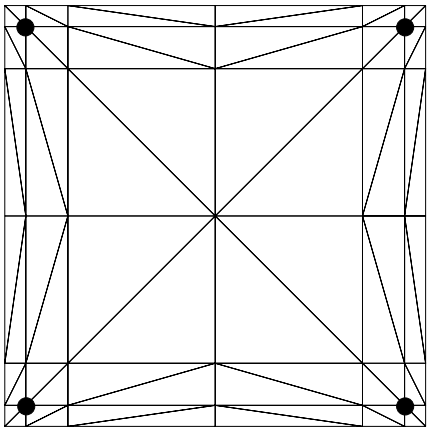

Geometry:	
Length	$L = 10.0$
Thickness	$h = 0.1$
Material properties:	
Young's modulus	$E = 35000.0$
Poisson's ratio	$\nu = 0.3$
Mass density	$\rho = 50.0$
● Fixed nodes	

Fig. 8. Definition of the plate test problem and a typical mesh used in the calculations.

which can be expressed more formally as:

$$\min_{\boldsymbol{s}} \quad \sum_{l=1}^{L} \sum_{m=1}^{L} \boldsymbol{u}_l \boldsymbol{K}^{lm} \boldsymbol{u}_m \tag{11}$$

where $\boldsymbol{s}$ is the set of design variables, L is the number of nodes, $\boldsymbol{u}_l$ is the vector of vertex displacements, and $\boldsymbol{K}^{lm}$ is the stiffness matrix. Although not explicitly indicated in (eq. 11), the stiffness matrix and the displacements depend on the design variables. Furthermore, the range of the design variables $\boldsymbol{s}$ is provided by the user. Within the subdivision framework the vertices of the control mesh are the design variables. For the plate example we chose as design variables the out of plane components of the control vertice positions in Figure 8. In order to compute the stiffness in (eq. 11) during the design space exploration we utilize the finite-element method based on the shape functions induced by subdivision as described earlier. However, the resolution of the control mesh is not sufficient for finite-element analysis. The control mesh is subdivided twice prior to the computation (Figure 9, left). Using the finite-element mesh vertices directly as design variables would lead to too many unknowns during the optimization procedure. In addition it leads to oscillations in the optimized shape so that the results of the optimization are useless (11). Consequently the parameters of the CAD model are chosen as the optimization variables. In a traditional framework this requires the generation of a finite-element mesh separate from the original CAD model, bringing with it the computational disadvantage of keeping two representations. The subdivision based approach is computationally efficient and representationally unified way to use the subdivision control mesh to parameterize both the geometry and the finite-element model.

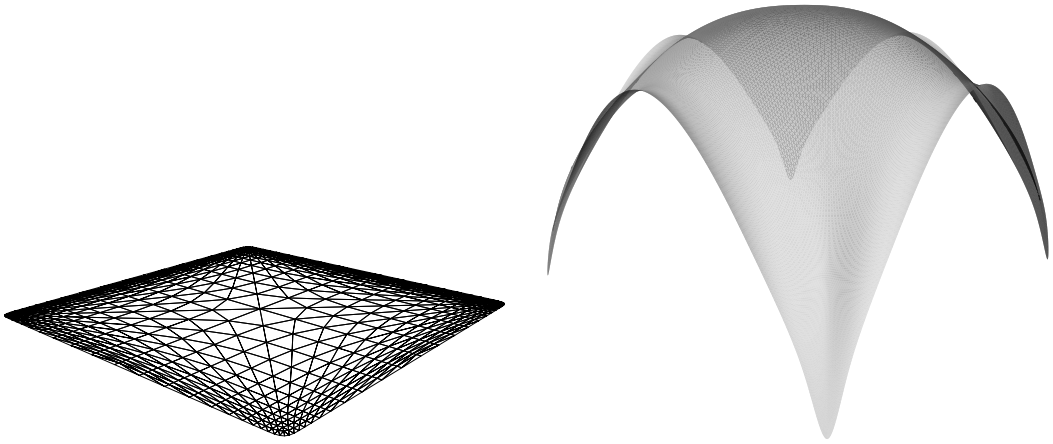

Finite-element mesh Optimum shape

Fig. 9. Square plate example.

The optimized roof structure is shown in Figure 9. For thin-shells the response to membrane strain is much stiffer than response to bending strain. Accordingly, the stiffness of the initial flat plate with bending energy only can be increased by changing the initial geometry of the shell as shown in Figure 9. Note the small features close to the free boundaries of the optimized shape. Through the optimization process the objective function in (eq. 11) could be minimized from 22541.32 to 55.39. This improvement demonstrates the well known strong influence of the curvature on structural stiffness.

5.2 VW Hood

As a second illustration of the value of the multiresolution simulation method using subdivision surfaces, consider the *circa*-1960 VW Beetle hood shown in Figure 10. The engineering design problem for the VW hood is to select a geometry of the hood to obtain superior performance in a number of aspects of performance, both measured and unmeasured. Chief among these performance concerns is a measure of torsional stiffness (the hood should not deform unacceptably if lifted from a point off-center at the front), which will be computed using the finite-element method based on the shape functions induced by subdivision. In addition, the total weight and the storage volume under the hood are calculated, and the styling, manufacturability, and usability of the hood are taken into account.

The original surface model (Figure 10) has 63 control points. There are 28 reflected pairs, leaving 35 unique control points if symmetry is enforced. Of those 35 points, 12 lie on the edge of the hood, and as the hood boundary is presumed to be fixed, those 12 points are fixed as well. It would be possible to treat the 23 remaining control points as design variables, and vary them

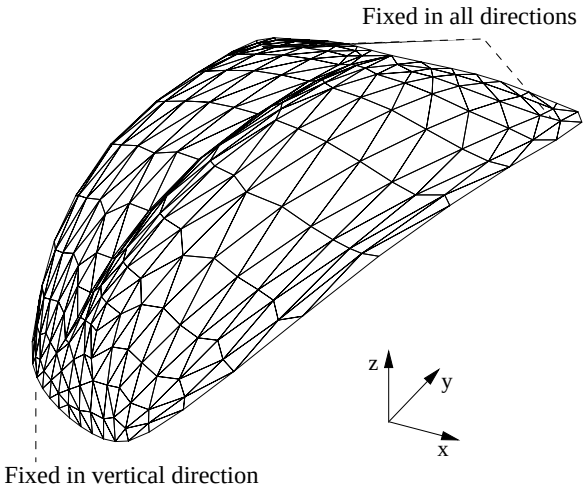

Geometry :	
$\max x - \min x$	$= 40.79$
$\max y - \min y$	$= 42.03$
$\max z - \min z$	$= 26.36$
Thickness	$= 0.12$
Material :	
Young's modulus	$E = 12500$
Poisson's ratio	$\nu = 0.290$
Mass density	$\rho = 0.1$

Fig. 10. Definition of the hood problem.

individually. In order to lessen deviations from the original styling (the hood ought to look like a VW), these 23 control points are varied using four non-dimensional geometric parameters: the swell of the hood (Figure 11, left), the depth of the characteristic center crease (Figure 11, right), the swell of the upper portion of each side of the hood (Figure 12, right), and the swell of the lower portion of each side of the hood (Figure 12, left). At the reference configuration all design variables have a value of one, and at zero all curves flatten to straight lines.

As mentioned, the design problem for the VW hood is not one of simple optimization. Since the finite-element mesh is easily modified, it is possible to "optimize" the design variables for minimum weight (Figure 13, left), or maximum stiffness (Figure 13, right). These "optima" may be undesirable for other reasons such as styling or manufacturability; also, one may sacrifice too much stiffness to achieve the lightest possible design, or vice versa. Using the lowest resolution finite-element analysis and an iterative search process, an approximate Pareto frontier on trade-offs between weight and stiffness can be found. As shown in Figure 14, there are many Pareto points, many of which significantly outperform the reference configuration in both weight and stiffness. Acquisition of the approximate Pareto frontier is made possible by use of the fastest (coarsest) analysis; when a smaller region of design space is explored at the next design iteration, a finer, more accurate finite-element analysis can be employed.

The search for desirable designs can be further hastened by the use of approximations (which were not used in this example), and by *a priori* analysis of the trade-offs between performance measures. By determining trade-off strategies and weights as described in (28), it is possible to search directly for a solution to fulfill a desired level of trade-off and relative importance weighting among the attributes. One such solution, representing a relatively non-compensating

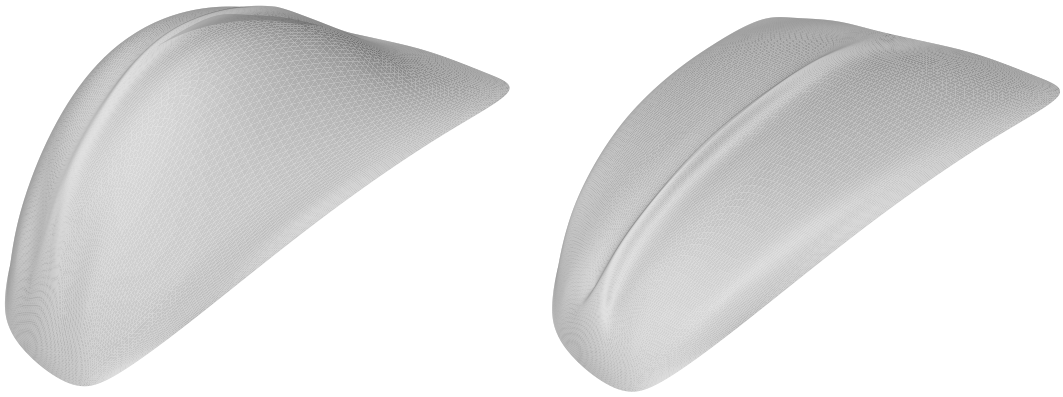

Center swell Crease

Fig. 11. VW hood variations.

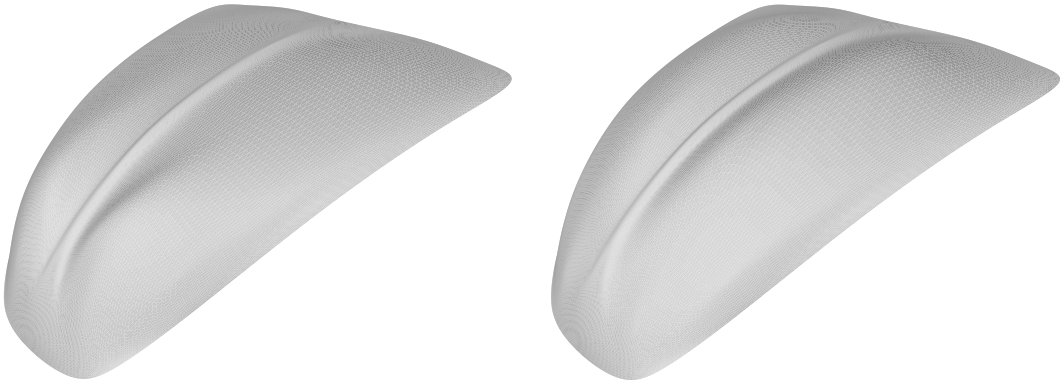

Lower side swell Upper side swell

Fig. 12. VW hood variations.

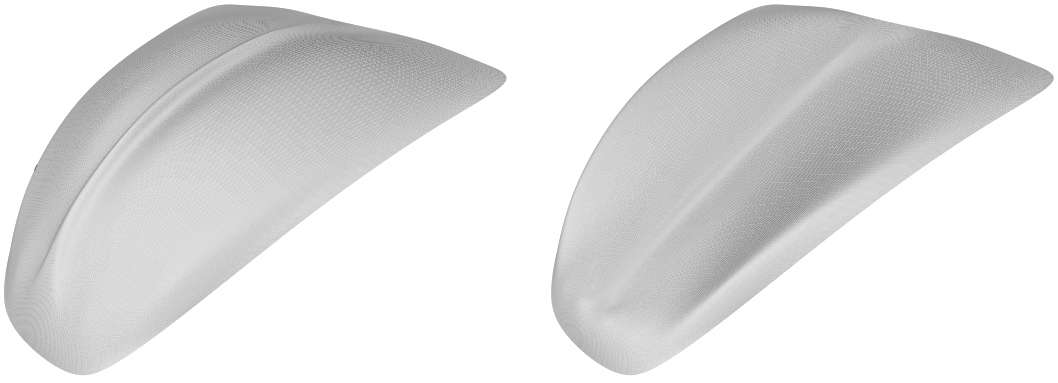

Optimized with respect to weight Optimized with respect to stiffness

Fig. 13. Optimized VW hood.

trade-off ($s = -10$), is shown in Figure 15, which appears as a black triangle in Figure 14. This particular solution is relatively insensitive to deviations from equal importance weights for the two attributes, and does not differ much

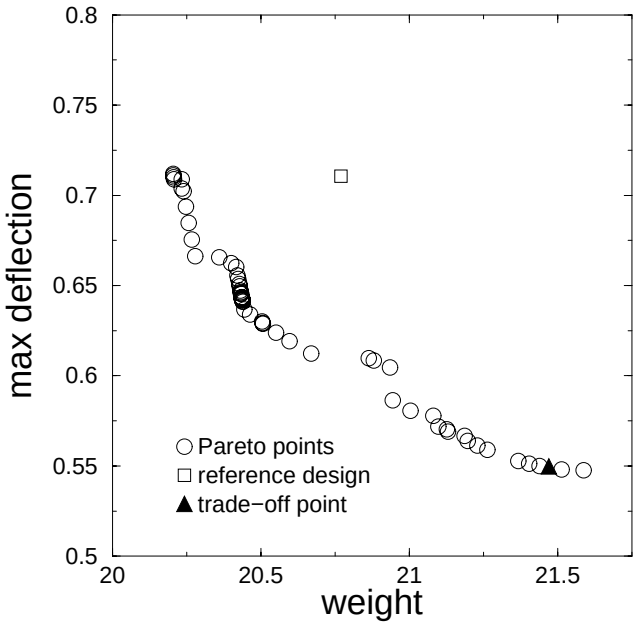

Fig. 14. VW hood: Pareto frontier

Fig. 15. VW hood: Trade-off.

from the minimum weight solution. As was shown in (28), every point on the Pareto frontier is the optimum for some trade-off strategy and pair of weights, so different decision analyses could lead to different solutions. In any case, the amount of necessary computation is greatly reduced by choosing importance weighting and a degree of compensation between attributes in advance (28).

6 Summary and Conclusions

We have proposed subdivision surfaces as a common foundation for modeling, simulation, and design in a unified framework. Subdivision surfaces provide a flexible and efficient tool for arbitrary topology free-form surface modeling, avoiding many of the problems inherent in traditional spline patch based approaches. In addition, the underlying basis functions are ideally suited to the finite-element analysis of thin-shells. The resulting solvers are highly scalable, providing an efficient computational foundation for design exploration and optimization. In particular, the ability to represent smooth surfaces with a relatively coarse control mesh greatly facilitates geometric optimization. The examples of application presented here illustrate the versatility and effectiveness of this paradigm.

Acknowledgements

Special thanks to Leif Kobbelt, Max-Planck-Institut für Informatik, Saarbrücken, and the SGI-Utah Visual Supercomputing Center. The support of DARPA and NSF through Caltech's OPAAL Project (DMS-9875042) is gratefully acknowledged. Additional support was provided by NSF under grant numbers: ACI-9624957, ACI-9721349, ASC-8920219, DMI-9523232, DMI-9813121, through a Packard fellowship to PS, and by Alias|Wavefront. Any opinions, findings, conclusions, or recommendations expressed in this publication are those of the authors and do not necessarily reflect the views of the sponsors.

References

[1] Ahmad, S., Irons, B., and Zienkiewicz, O. Analysis of Thick and Thin Shell Structures by Curved Finite Elements. *Internat. J. Numer. Methods Engrg. 2* (1970), 419–451.

[2] Alias|Wavefront. *Maya, 3.0*. Toronto.

[3] Antonsson, E. K., and Otto, K. N. Imprecision in engineering design. *ASME Journal of Mechanical Design 117(B) (Special Combined Issue of the Transactions of the ASME commemorating the 50th anniversary of the Design Engineering Division of the ASME.)* (June 1995), 25–32. Invited paper.

[4] Biermann, H., Levin, A., and Zorin, D. Piecewise Smooth Subdivision Surfaces with Normal Control. In *Computer Graphics (SIGGRAPH '00 Proceedings)*, 113–120, 2000.

[5] Bletzinger, K., and Ramm, E. Form Finding of Shells by Structural Optimization. *Engng. Comput.* (9 1993), 27–35.

[6] Catmull, E., and Clark, J. Recursively Generated B-Spline Surfaces on Arbitrary Topological Meshes. *Comput. Aided Design 10*, 6 (1978), 350–355.

[7] Cirak, F., and Ortiz, M. Fully C^1-Conforming Subdivision Elements for Finite Deformation Thin-Shell Analysis. *In press, Internat. J. Numer. Methods Engrg.* (2000).

[8] Cirak, F., Ortiz, M., and Schröder, P. Subdivision Surfaces: A New Paradigm for Thin-Shell Finite-Element Analysis. *Internat. J. Numer. Methods Engrg. 47* (2000), 2039–2072.

[9] Doo, D., and Sabin, M. Behaviour of Recursive Division Surfaces Near Extraordinary Points. *Comput. Aided Design 10*, 6 (1978), 356–360.

[10] Green, A., and Zerna, W. *Theoretical Elasticity*, 2 ed. Oxford University Press, England, 1968.

[11] Haftka, R., and Grandhi, R. Structural Shape Optimization - A Survey. *Comput. Methods Appl. Mech. Engrg. 57* (1986), 91–106.

[12] Halstead, M., Kaas, M., and DeRose, T. Efficient, Fair Interpolation using Catmull-Clark Surfaces. In *Computer Graphics (SIGGRAPH '93 Proceedings)*, 1993.

[13] Hsieh, C., and Oh, K. MARS: A computer-based method for achieving robust systems. In *The Integration of Design and Manufacture, Volume I*, 115–120, June 1992.

[14] Kagan, P., Fischer, A., and Bar-Yoseph, P. Integrated Mechanically Based CAE System. In *Proceedings of Fifth Symposium on Solid Modeling and Applications*, W. Bronsvoort and D. Anderson, Eds., 23–30, June 1999.

[15] Keeney, R., and Raiffa, H. *Decisions with multiple objectives: Preferences and value tradeoffs*. Cambridge University Press, Cambridge, U.K., 1993.

[16] Khodakovsky, A., and Schröder, P. Fine Level Feature Editing

for Subdivision Surfaces. In *Proceedings of Fifth Symposium on Solid Modeling and Applications*, W. Bronsvoort and D. Anderson, Eds., 203–211, June 1999.

[17] Kobbelt, L., Hesse, T., Prautzsch, H., and Schweizerhof, K. Iterative Mesh Generation for FE-Computations on Free Form Surfaces. *Engng. Comput. 14* (1997), 806–820.

[18] Langner, W. J. Sensitivity analysis and optimization of mechanical system design. In *Advances in Design Automation - 1988*, S. S. Rao, Ed., vol. DE-14, 175–182, Sept. 1988.

[19] Levin, A. Combined Subdivision Schemes for the Design of Surfaces Satisfying Boundary Conditions. *Computer Aided Geometric Design 16* (1999), 345–354.

[20] Loop, C. Smooth Subdivision Surfaces Based on Triangles. Master's thesis, University of Utah, Department of Mathematics, 1987.

[21] Mandal, C., Qin, H., and Vemuri, B. A Novel FEM-Based Dynamic Framework for Subdivision Surfaces. In *Proceedings of Fifth Symposium on Solid Modeling and Applications*, W. Bronsvoort and D. Anderson, Eds., 191–202, June 1999.

[22] Montgomery, D. C. *Design and analysis of experiments*. J. Wiley and Sons, New York, NY, 1991.

[23] Naghdi, P. *Handbuch der Physik, Mechanics of Solids II*, vol. VI a/2. Springer, Berlin, 1972, ch. The theory of shells.

[24] Olhoff, N., Bendsoe, M., and Rasmussen, J. On CAD-Integrated Structural Topology and Design Optimization. *Comput. Methods Appl. Mech. Engrg. 89* (1991), 259–279.

[25] Otto, K. N., and Antonsson, E. K. Trade-off strategies in engineering design. *Research in Engineering Design 3*, 2 (1991), 87–104.

[26] Papalambros, P., and Wilde, D. *Principles of optimal design*. Cambridge University Press, Cambridge, U.K., 1988.

[27] Reif, U., and Schröder, P. Curvature Smoothness of Subdivision Surfaces. Tech. Rep. TR-00-03, California Institute of Technology, 2000.

[28] Scott, M. *Formalizing Negotiation in Engineering Design*. PhD thesis, California Institute of Technology, Pasadena, CA, June 1999.

[29] Scott, M. J., and Antonsson, E. K. Aggregation functions for engineering design trade-offs. In *9th International Conference on Design Theory and Methodology*, vol. 2, 389–396, Sept. 1995.

[30] Simpson, T. W., Peplinski, J., Koch, P. N., and Allen, J. K. On the use of statistics in design and the implications for deterministic computer experiments. In *9th International Conference on Design Theory and Methodology*, sep 1997.

[31] Stam, J. Fast Evaluation of Catmull-Clark Subdivision Surfaces at Arbitrary Parameter Values. In *Computer Graphics (SIGGRAPH '98 Proceedings)*, 1998.

[32] Stam, J. Fast Evaluation of Loop Triangular Subdivision Surfaces at Arbitrary Parameter Values. In *Computer Graphics (SIGGRAPH '98*

Proceedings, CD-ROM supplement), 1998.

[33] Strang, G., and Fix, G. J. *An Analysis of the Finite Element Method*. Prentice-Hall, Englewood Cliffs, N.J., 1973.

[34] von Neumann, J., and Morgenstern, O. *Theory of games and economic behavior*, 2nd ed. Princeton University Press, Princeton, NJ, 1953.

[35] Ward, A. C., Liker, J. K., Sobek, D. K., and Cristiano, J. J. The second Toyota paradox: How delaying decisions can make better cars faster. *Sloan Management Review 36*, 3 (Spring 1995), 43–61.

[36] Wood, K. L., and Antonsson, E. K. Computations with imprecise parameters in engineering design: Background and theory. *ASME Journal of Mechanisms, Transmissions, and Automation in Design 111*, 4 (Dec. 1989), 616–625.

[37] Zorin, D., and Schröder, P., Eds. *Subdivision for Modeling and Animation* (1999), Computer Graphics (SIGGRAPH '99 Course Notes).